

Measuring the angle α_{ds} of the flattest Unitary Triangle with $\bar{B}_d \rightarrow \phi \bar{K}^{(*)0}$, $\bar{B}_s \rightarrow \phi K^{(*)0}$ decays

R. Aleksan¹, L. Oliver², E. Perez³

¹IRFU, CEA, Université Paris-Saclay, 91191 Gif-sur-Yvette cedex, France

²IJCLab, Pôle Théorie, CNRS/IN2P3 et Université Paris-Saclay,

Bât. 210, 91405 Orsay cedex, France

³CERN, EP Department, Geneva, Switzerland

February 16, 2024

ABSTRACT

We show that the angle α_{ds} of the “flattest” unitarity triangle can be directly measured using the decays $\bar{B}_d \rightarrow \phi \bar{K}^{(*)0}$ and $\bar{B}_s \rightarrow \phi K^{(*)0}$. Using both \bar{B}_d and \bar{B}_s enables a further consistency test since the expected time-dependent CP violating asymmetries are identical though with opposite signs. Since large statistics of \bar{B}_d and \bar{B}_s are needed for accurate measurements, FCC-ee and its environment at the Z-pole is well suited for such studies. These measurements, the precision of which could reach the sub-degree level, will contribute to probe further the consistency of the CP sector of the Standard Model with unprecedented level of accuracy. The main detector requirements that are set by these measurements are also outlined.

1 Introduction

The very high statistics anticipated at FCC-ee [1, 2, 3] open new possibilities for studying Flavor Physics and CP violation. An endeavor that can be taken over with the FCC statistics at the Z-pole, where more than $5 \cdot 10^{12}$ Z bosons should be accumulated, would be to probe with an unprecedented accuracy the CP sector of the Standard Model (SM) and to measure directly as many angles of the CKM unitary triangles. In recent papers, we have proposed to measure directly the 3 angles of a flat unitarity triangle [4, 5]. In the present paper we propose to measure one of the angles of the flattest unitarity triangle.

2 Definition of the Unitary Angles

In the SM, one derives the unitarity relations from the CKM quark mixing matrix [6],

$$V_{CKM} = \begin{bmatrix} V_{ud} & V_{us} & V_{ub} \\ V_{cd} & V_{cs} & V_{cb} \\ V_{td} & V_{ts} & V_{tb} \end{bmatrix} \quad (1)$$

Should there be only 3 families of quarks, the unitarity relations, which are derived from $V_{CKM}V_{CKM}^{-1} = 1$, read as below:

$$\begin{aligned} UT_{db} &\equiv V_{ub}^*V_{ud} + V_{cb}^*V_{cd} + V_{tb}^*V_{td} = 0 \\ UT_{sb} &\equiv V_{ub}^*V_{us} + V_{cb}^*V_{cs} + V_{tb}^*V_{ts} = 0 \\ UT_{ds} &\equiv V_{us}^*V_{ud} + V_{cs}^*V_{cd} + V_{ts}^*V_{td} = 0 \end{aligned} \quad (2)$$

In Equation 2, only 3 relations have been displayed and are visualized in Figure 1. There are also 3 additional ones, but they are very similar to those above. In the SM, the CKM matrix has only 4 independent parameters. Therefore the angles of all these triangles can be expressed in terms of 4 angles [7]. The first relation in Equation 2 is known as the Unitarity Triangle, with the 3 sides of the same order, and has been studied extensively. However the other ones would deserve to be studied in detail as well in order to investigate further the consistency of the SM. We define the angles of these triangles as

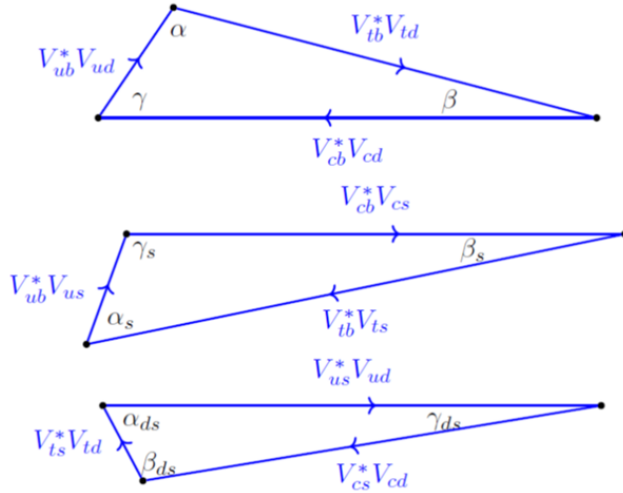


Figure 1: Unitarity Triangle UT_{db} involving the 1st and 3rd columns (top), Unitarity Triangle UT_{sb} involving the 2nd and 3rd columns (center) and Unitarity Triangle UT_{ds} involving the 1st and 2nd columns (bottom) of the CKM matrix. Note that these triangles are not to scale.

$$\alpha = \arg\left(-\frac{V_{tb}^*V_{td}}{V_{ub}^*V_{ud}}\right), \beta = \arg\left(-\frac{V_{cb}^*V_{cd}}{V_{tb}^*V_{td}}\right), \gamma = \arg\left(-\frac{V_{ub}^*V_{ud}}{V_{cb}^*V_{cd}}\right) \quad (3)$$

$$\alpha_s = \arg\left(-\frac{V_{ub}^* V_{us}}{V_{tb}^* V_{ts}}\right), \beta_s = \arg\left(-\frac{V_{tb}^* V_{ts}}{V_{cb}^* V_{cs}}\right), \gamma_s = \arg\left(-\frac{V_{cb}^* V_{cs}}{V_{ub}^* V_{us}}\right) \quad (4)$$

$$\alpha_{ds} = \arg\left(-\frac{V_{us}^* V_{ud}}{V_{ts}^* V_{td}}\right), \beta_{ds} = \arg\left(-\frac{V_{ts}^* V_{td}}{V_{cs}^* V_{cd}}\right), \gamma_{ds} = \arg\left(-\frac{V_{cs}^* V_{cd}}{V_{us}^* V_{ud}}\right) \quad (5)$$

For the angles α , β , γ of the triangle UT_{db} we have adopted the usual convention with circular permutation of the quarks t , c , u . For the triangle UT_{sb} , we have adopted the generally accepted notation for β_s in [8] and for the other angles the corresponding circular permutations of t , c , u . For the triangle UT_{ds} , we have used the notation of UT_{sb} with the replacement $b \rightarrow s$, $s \rightarrow d$. This latter triangle is the flattest one since the angle γ_{ds} is almost π . Measuring directly this angle is very difficult, however it is possible, as we will show here, to measure α_{ds} with some specific B decays.

3 $B_{d,s} \rightarrow \phi K^{*0}(\bar{K}^{*0})$ or $B_{d,s} \rightarrow \phi K_s$

These decays are pure penguin decays, i.e. no tree diagrams, either color allowed or suppressed, are possible. Figure 2 show the main diagrams.

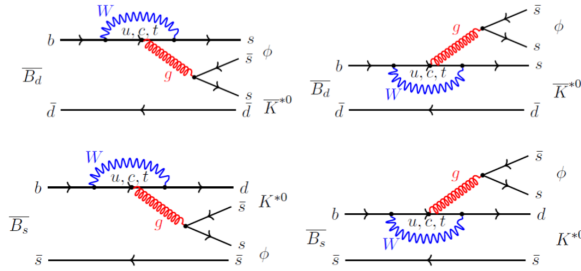


Figure 2: $\bar{B}_{d,s} \rightarrow \phi K^{*0}(\bar{K}^{*0})$ decay diagrams. The diagrams for $B_{d,s} \rightarrow \phi K_s$ are identical. Not shown here, there are also annihilation diagrams, which are however subleading.

Let us concentrate on the case where the $K^{*0}(\bar{K}^{*0})$ decays to the CP eigenstates $K_s\pi^0$. Then both $B_{d,s}$ and $\bar{B}_{d,s}$ can decay to the final state and therefore CP violation occurs through $B - \bar{B}$ mixing.

$$|B_{L(H)} = p|B_{d,s} \rangle + (-)q|\bar{B}_{d,s} \rangle \quad (6)$$

In the Standard Model, the box diagrams in Figure 3, which are responsible for $B_s - \bar{B}_s$ mixing, are overwhelmingly dominated by the t -quark exchange. Thus one can safely use the approximation $|q/p|_{B_s} \simeq 1$, where q/p is given by a ratio of CKM elements $V_{tb}^* V_{ts}$. This approximation is good at the sub per mille level. Similar diagrams are involved for $B_d - \bar{B}_d$ mixing and thus one obtains $|q/p|_{B_d} \simeq 1$, where q/p is given by a ratio of CKM elements $V_{tb}^* V_{td}$.

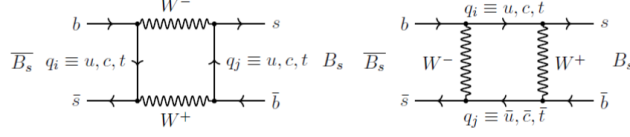


Figure 3: The box Feynman diagrams for the $\overline{B}_s - B_s$ mixing. The mixing is dominated by t -quark exchange. Similar diagrams are involved for $\overline{B}_d - B_d$ mixing, in which the s -quark is replaced by a d -quark.

$$\left(\frac{q}{p}\right)_{B_s} = - \left(\sqrt{\frac{M_{12}^*}{M_{12}}}\right)_{B_s} \simeq -\frac{V_{tb}^* V_{ts}}{V_{tb} V_{ts}^*} \quad (7)$$

and

$$\left(\frac{q}{p}\right)_{B_d} = - \left(\sqrt{\frac{M_{12}^*}{M_{12}}}\right)_{B_d} \simeq -\frac{V_{tb}^* V_{td}}{V_{tb} V_{td}^*} \quad (8)$$

$$\lambda_{d,s}(f) = \left(\frac{q}{p}\right)_{B_{d,s}} \frac{\langle f | \overline{B}_{d,s} \rangle}{\langle f | B_{d,s} \rangle}, \quad \overline{\lambda}_{d,s}(f) = \left(\frac{p}{q}\right)_{B_{d,s}} \frac{\langle f | B_{d,s} \rangle}{\langle f | \overline{B}_{d,s} \rangle} \quad (9)$$

writing $\rho_{d,s} = |\lambda_{d,s}(f)|$ and assuming top dominance, one has

$$\lambda_{d,s}(f) = \rho_{d,s} e^{i(\phi_{CKM})}, \quad \overline{\lambda}_{d,s}(f) = \frac{1}{\rho_{d,s}} e^{-i(\phi_{CKM})} \quad (10)$$

where ϕ_{CKM} is the CKM phase.

The time dependent distributions for these decays read :

$$\begin{aligned} \Gamma(\overline{B}_q(t) \rightarrow f) &= N_{q,f} |A_{q,f}|^2 \left[\frac{1+\rho_q^2}{2}\right] e^{-\Gamma_q t} \times \\ &\left[\cosh \frac{\Delta\Gamma_q t}{2} - A_{CP}^{dir} \cos(\Delta m_q t) + A_{\Delta\Gamma_q} \sinh \frac{\Delta\Gamma_q t}{2} - A_{CP}^{mix} \sin(\Delta m_q t) \right] \\ \Gamma(B_q(t) \rightarrow f) &= N_{q,f} |A_{q,f}|^2 \left[\frac{1+\rho_q^2}{2}\right] e^{-\Gamma_q t} \times \\ &\left[\cosh \frac{\Delta\Gamma_q t}{2} + A_{CP}^{dir} \cos(\Delta m_q t) + A_{\Delta\Gamma_q} \sinh \frac{\Delta\Gamma_q t}{2} + A_{CP}^{mix} \sin(\Delta m_q t) \right] \end{aligned} \quad (11)$$

with

$$A_{CP}^{dir} = \frac{1-\rho_q^2}{1+\rho_q^2}, \quad A_{\Delta\Gamma_q} = -\frac{2Re\lambda_{q,f}}{1+\rho_q^2}, \quad A_{CP}^{mix} = -\frac{2Im\lambda_{q,f}}{1+\rho_q^2} \quad (12)$$

For the decays $\overline{B}_{d,s} \rightarrow \phi(K_s \pi^0)_{K^*0}$, the product of the CKM elements is invariant. Namely with top dominance, one gets for B_s :

$$\begin{aligned} -\frac{V_{tb}^* V_{ts}}{V_{tb} V_{ts}^*} \times \frac{V_{tb} V_{td}^*}{V_{tb}^* V_{td}} \times \frac{V_{us}^* V_{ud}}{V_{us} V_{ud}^*} &= -\frac{V_{ud} V_{us}^*}{V_{td} V_{ts}^*} \times \frac{V_{td}^* V_{ts}}{V_{ud}^* V_{us}} \\ &= \left| \frac{V_{ud} V_{us}^*}{V_{td} V_{ts}^*} \right| \times \left| \frac{V_{td}^* V_{ts}}{V_{ud}^* V_{us}} \right| e^{i\phi_{CKM}} \end{aligned} \quad (13)$$

with

$$\phi_{CKM} = \pi + 2\alpha_{ds} \quad (14)$$

similarly, one gets for B_d :

$$\begin{aligned}
& -\frac{V_{tb}^*V_{td}}{V_{tb}V_{td}^*} \times \frac{V_{tb}V_{ts}^*}{V_{tb}^*V_{ts}} \times \frac{V_{ud}^*V_{us}}{V_{us}V_{ud}^*} = -\frac{V_{us}V_{ud}^*}{V_{ts}V_{td}^*} \times \frac{V_{ts}^*V_{td}}{V_{us}^*V_{ud}} \\
& = \left| \frac{V_{us}V_{ud}^*}{V_{ts}V_{td}^*} \right| \times \left| \frac{V_{ts}^*V_{td}}{V_{us}^*V_{ud}} \right| e^{i\phi_{CKM}}
\end{aligned} \tag{15}$$

with

$$\phi_{CKM} = \pi - 2\alpha_{ds} \tag{16}$$

Therefore with both \bar{B}_s and \bar{B}_d decays to $\phi K^{*0}(\bar{K}^{*0})$, where $K^{*0}(\bar{K}^{*0})$ decays to $K_s\pi^0$, one measures the angle α_{ds} of the 3rd Unitarity Triangle in Fig. 1. The same result is obtained with the decays ϕK_s . With top dominance, the sum of the CKM phases for $\bar{B}_s \rightarrow \phi K_s$ and $\bar{B}_d \rightarrow \phi K_s$ is 2π . *It is therefore very important to make this measurement with both B_s and B_d .* This will enable to be sensitive to new physics if the results show different values for α_{ds} .

Note also that if unitarity with 3 families holds, as in the SM, one has

$$\alpha_{ds} = \beta + \beta_s - \gamma_{ds} \tag{17}$$

It is thus an indirect measurement of β_s since $\beta - \gamma_{ds}$ is known from the process $\bar{B}_d \rightarrow J/\psi K_s$. This indirect measurement is not competitive with the direct measurement using $\bar{B}_s \rightarrow J/\psi\phi$, however it allows to check the consistency of the SM.

3.1 Expectation with QCD Factorization

Table 1 shows the experimental data for the modes $\bar{B}_d \rightarrow \phi \bar{K}^{(*)0}$, $\bar{B}_s \rightarrow \phi K^{(*)0}$.

B decay	Br($\times 10^{-6}$)	f_L	f_{\parallel}	f_{\perp}
$\bar{B}^0 \rightarrow \bar{K}^0\phi$	7.3 ± 0.7	n/a	n/a	n/a
$\bar{B}^0 \rightarrow \bar{K}^{*0}\phi$	10.0 ± 0.5	0.497 ± 0.017	<i>0.279 ± 0.023</i>	0.224 ± 0.015
$\bar{B}_s \rightarrow \phi K^0$	$1.3 \pm 0.6^*$	n/a	n/a	n/a
$\bar{B}_s \rightarrow \phi K^{*0}$	1.14 ± 0.30	0.51 ± 0.17	0.21 ± 0.11	<i>0.28 ± 0.20</i>

Table 1: Branching fractions, f_L , f_{\parallel} and f_{\perp} from the PDG [8]. f_L , f_{\parallel} and f_{\perp} are the longitudinal, parallel and perpendicular polarization fractions, respectively. Statistical and systematic errors have been added in quadrature. The values in italic are not measured directly but are deduced from $f_L + f_{\parallel} + f_{\perp} = 1$. *This Branching fraction includes all $K^+K^-K^0$ decays.

In $\bar{B} \rightarrow V_1V_2$ decays, one is dealing with 3 helicity amplitudes.

$$\bar{\mathcal{A}}_0 = A[\bar{B} \rightarrow V_1(0)V_2(0)] \quad , \quad \bar{\mathcal{A}}_{\pm} = A[\bar{B} \rightarrow V_1(\pm)V_2(\pm)] \tag{18}$$

Moving from the helicity representation to the transversity one, one

gets :

$$\bar{\mathcal{A}}_L \equiv \bar{\mathcal{A}}_0 \quad (19)$$

$$\bar{\mathcal{A}}_{\parallel} = \frac{\bar{\mathcal{A}}_+ + \bar{\mathcal{A}}_-}{\sqrt{2}} \quad , \quad \bar{\mathcal{A}}_{\perp} = \frac{\bar{\mathcal{A}}_+ - \bar{\mathcal{A}}_-}{\sqrt{2}}$$

with the corresponding transversity rate fractions f_L , f_{\parallel} and f_{\perp} satisfying

$$f_L + f_{\parallel} + f_{\perp} = 1 \quad (20)$$

At $q^2 = 0$ and in the heavy quark limit and large recoil energy for the light meson,

$$\bar{\mathcal{A}}_+ \simeq 0 \quad (21)$$

and one then has

$$\bar{\mathcal{A}}_{\parallel} \simeq -\bar{\mathcal{A}}_{\perp} \simeq \frac{\bar{\mathcal{A}}_-}{\sqrt{2}} \quad (22)$$

$$|\bar{\mathcal{A}}_{\parallel}|^2 + |\bar{\mathcal{A}}_{\perp}|^2 \simeq |\bar{\mathcal{A}}_-|^2 \equiv |\bar{\mathcal{A}}_T|^2$$

where the subindex T stands for transverse. Finally, in the SM ($V - A$), one gets

$$f_{\parallel} \simeq f_{\perp} \quad (23)$$

As can be seen in Table 1, equation (23) seems to be verified within experimental errors. We examine now whether $\phi_{L,\parallel,\perp}^{CKM}$ differ significantly when c, u quarks are considered in the loops using QCD Factorization [9]. As mentioned above, equations (13) and (15) hold exactly when top dominance is assumed. Table 2 shows the expected values for $\lambda_{L,\parallel,\perp}$ and $\phi_{L,\parallel,\perp}^{CKM}$ using QCD Factorization. As it can be observed, the measurement of $2\alpha_{d,s}$ still holds within the theoretical errors. However one notes also that $|\lambda_{L,\parallel,\perp}|$ is different from 1 for the decay $\bar{B}_s \rightarrow \phi K^{(*)0}$, due to the presence of direct CP violation effects. This is due to the fact that the CKM elements involved in the leading penguin diagram for the \bar{B}_s decay are of the same order, λ^3 , in contrast to the B_d , for which the dominant terms (with t and c exchange) are of order λ^2 while the other term (with u exchange) is of order λ^4 .

4 Detector simulation

4.1 Generic detector resolutions

We consider a typical FCC-ee detector in order to study the acceptance efficiency as well as the momentum, mass and vertex resolutions for the charged tracks. More precisely, a complete tracking simulation including multiple scattering is carried out for a large

Decay	$\overline{B}_d \rightarrow \phi \overline{K}^0$	$\overline{B}_d \rightarrow \phi \overline{K}^{*0}$	$\overline{B}_s \rightarrow \phi K^0$	$\overline{B}_s \rightarrow \phi K^{*0}$
$ \lambda_L $	1.017 ± 0.005	1.016 ± 0.005	0.743 ± 0.075	0.746 ± 0.069
ϕ_L^{CKM}	$\pi - 2\alpha_{\text{ds}} + 0.004 \pm 0.005$	$\pi - 2\alpha_{\text{ds}} + 0.003 \pm 0.006$	$\pi + 2\alpha_{\text{ds}} - 0.030 \pm 0.121$	$\pi + 2\alpha_{\text{ds}} - 0.021 \pm 0.105$
$ \lambda_{\parallel} $	–	1.005 ± 0.001	–	0.917 ± 0.021
$\phi_{\parallel}^{\text{CKM}}$	–	$\pi - 2\alpha_{\text{ds}} - 0.002 \pm 0.002$	–	$\pi + 2\alpha_{\text{ds}} - 0.028 \pm 0.035$
$ \lambda_{\perp} $	–	1.005 ± 0.001	–	0.917 ± 0.021
$\phi_{\perp}^{\text{CKM}}$	–	$\pi - 2\alpha_{\text{ds}} - 0.002 \pm 0.002$	–	$\pi + 2\alpha_{\text{ds}} - 0.028 \pm 0.035$

Table 2: The expected values of $|\lambda_{L,\parallel,\perp}|$ and $\phi_{L,\parallel,\perp}^{\text{CKM}}$ for \overline{B}_d and \overline{B}_s decays within QCD factorization.

set of momenta and polar angles to determine the momentum resolution and angular resolutions. For a fast simulation, we then parametrize the resolutions using this set of data. The energy and angular parametrization for photons and electrons assumes a crystal type electromagnetic calorimeter and we use typical conservative resolutions. In summary the detector resolutions are listed in (24),

Acceptance :	$ \cos \theta $	< 0.95	
Charged particles :			
p_T resolution :	$\frac{\sigma(p_T)}{p_T^2}$	$= 2. \times 10^{-5} \oplus$	$\frac{1.2 \times 10^{-3}}{p_T \sin \theta}$
ϕ, θ resolution :	$\sigma(\phi, \theta) \text{ } \mu\text{rad}$	$= 18 \oplus$	$\frac{1.5 \times 10^3}{p_T \sqrt[3]{\sin \theta}}$
Vertex resolution :	$\sigma(d_{\text{Im}}) \text{ } \mu\text{m}$	$= 1.8 \oplus$	$\frac{5.4 \times 10^1}{p_T \sqrt{\sin \theta}}$
e, γ particles :			
Energy resolution :	$\frac{\sigma(E)}{E}$	$= \frac{5 \times 10^{-2}}{\sqrt{E}} \oplus$	5×10^{-3}
EM ϕ, θ resolution :	$\sigma(\phi, \theta) \text{ mrad}$	$= \frac{7}{\sqrt{E}}$	

(24)

where θ, ϕ are the particles' polar and azimuthal angles respectively, p_T (in GeV) the track transverse momentum, E the e^\pm, γ energy and d_{Im} the tracks' impact parameter. In addition to this parameterised detector response, we have also used Monte-Carlo events processed through a DELPHES [10] simulation of the IDEA detector concept [3]; more details will be given in Section 5.2.

4.2 Vertex resolution at FCC-ee

The expected number of produced events at FCC-ee are listed in Table 3. In order to study CP violation one needs to carry out a time dependent measurement. It is therefore important to have a good vertex resolution, which is particularly critical for the B_s decays since the oscillation frequency is high. The B_s flight distance resolution at the Z-pole with a FCC detector has been studied in detail for the decay $B_s \rightarrow D_s^\pm K^\mp$ in earlier work [4] and one finds $\sim 20 \mu\text{m}$. However in the decay $\overline{B}_s \rightarrow \phi K^{(*)0}$, the $K^0(K^{*0})$ has to decay to $K_s(K_s\pi^0)$ and therefore the resolution on the \overline{B}_s decay vertex is determined by the ϕK_s vertex, which is less precise than the vertex $D_s^\pm K^\mp$ with $D_s^\pm \rightarrow \phi \pi^\pm$. We have therefore studied the resolution on the \overline{B}_s flight distance using the ϕ and the K_s . This study uses signal Monte-Carlo events with a $\overline{B}_s \rightarrow \phi K_s$ decay

$\int L = 150 \text{ ab}^{-1}$			
$\sigma(e^+e^- \rightarrow Z)$	number	$f(Z \rightarrow \overline{B}_d)$	$f(Z \rightarrow \overline{B}_s)$
nb	of Z		
~ 42.9	$\sim 6.4 \cdot 10^{12}$	0.06	0.0159

Decay	Final	Number of	Number of
Mode	State	\overline{B}_d decays	\overline{B}_s decays
CP eigenstates			
ϕK^0	$K^+K^-(\pi^+\pi^-)_{K_s}$	$\sim 4.9 \cdot 10^5$	$\sim 1.7 \cdot 10^4$
ϕK^{*0}	$K^+K^-(\pi^+\pi^-)_{K_s}\pi^0$	$\sim 2.1 \cdot 10^5$	$\sim 6.4 \cdot 10^3$

Table 3: The expected number of produced \overline{B}_d and \overline{B}_s decays to specific modes at FCC-ee at a center of mass energy of 91 GeV over 5 years with 2 detectors. These numbers have to be multiplied by 2 when including B_d and B_s decays. The branching fractions of the PDG [8] have been used whenever available, else the expectation from QCD factorization is used.

processed through DELPHES, and a vertexing software [11, 12] that handles both charged and neutral particles. An average resolution of $70\mu m$ is found, see Figure 4. This resolution is, as expected, worse than the $20\mu m$ found with the full vertex information in the $B_s \rightarrow D_s^\pm K^\mp$ decays. This is due to the fact that the 2 Kaons from the ϕ -meson are produced with a small momentum (127 MeV/c) in the ϕ center of mass and they are emitted close to each other. The addition of the K_s improves significantly the resolution as it would be $168\mu m$ should one use only the ϕ . We remind nevertheless that the average B_s flight distance is $3mm$, hence the resolution of $70\mu m$ is excellent and does not significantly dilute the oscillations.

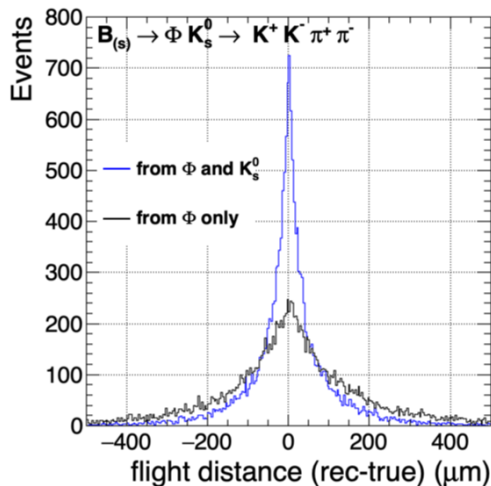


Figure 4: The resolution on the \overline{B}_s flight distance using the vertex $\phi - K_s$

5 Background studies

The final state ϕK^0 includes 2 charged kaons and a K_s while the final state ϕK^{*0} includes in addition a π^0 . Thanks to the excellent PID and the excellent momentum resolution, which are foreseen at the FCC-ee detectors, it is expected that these modes are essentially background free. We have nevertheless verified this using some exclusive final states processed with the parameterised detector response (Section 5.1), as well as generic $Z \rightarrow b\bar{b}, c\bar{c}$ events generated with PYTHIA and simulated with DELPHES (Section 5.2).

5.1 Exclusive final states

There are 3 main categories of exclusive final states that could potentially contribute to the background :

1. Final states with light mesons without long live particles (e.g. K_s or Λ) such as $\phi\rho^0 \rightarrow (K^+K^-)_\phi(\pi^+\pi^-)_{\rho^0}$ or $\phi f_0(980) \rightarrow (K^+K^-)_\phi(\pi^+\pi^-)_{f_0(980)}$
2. Final states with long live particles (e.g. K_s or Λ) such as $K^{*0}\bar{K}^0 + cc$ or $\Lambda\phi$
3. Final states with D_s^\pm particles decaying to $\phi\pi^\pm$ such as $D_s^\pm\pi^\mp$

The background in the first category is abundant but can be easily rejected by requiring the $\pi^+\pi^-$ mass to be around the K^0 mass and its vertex to be detached from the $(K^+K^-)_\phi$ vertex. This is discussed above in the vertexing section. This requirement rejects essentially all of this background, it also rejects part of the combinatoric background.

In the second category, the exclusive final states considered are $B_{d,s} \rightarrow K^{*0}K_s + cc$, $B_s \rightarrow K_2^{*0}(1430)K_s \rightarrow K^{*0}\pi^0 K_s + cc$, and $B_{d,s} \rightarrow K^{*0}\bar{K}^{*0}$ in which one of the K^{*0} or \bar{K}^{*0} decays to $K_s\pi^0$ while the other decays to $K^\pm\pi^\mp$. We have also included the decay $\Lambda_b \rightarrow \Lambda\phi$. These modes include a charged π or a proton and therefore are not a background, should one have a good Particle Identification (PID) system. Nevertheless, let us assume for now that one does not use PID. We show in Figure 5 the reconstructed mass of the final state $\bar{B}_{d,s} \rightarrow \phi K_s$, i.e. with a wrong assignment of the pion (proton) as a kaon (pion).

The mass resolution of the ϕK_s system is better than 9 MeV. It can be seen that as soon as the mass constraint is used for the ϕ and the K_s , essentially all background disappears and we are left with clear peaks for $\bar{B}_{d,s}$. Needless to say, should one have a PID system, these exclusive backgrounds would disappear as well, even without cutting on the ϕ or K_s mass.

Finally let us consider the third category, which is potentially dangerous since the final set of particles, $\phi\pi^+\pi^-$, is identical to the one in ϕK_s . Indeed the expected rate for $B_s \rightarrow D_s^\pm\pi^\mp \rightarrow \phi\pi^\pm\pi^\mp$ is about 400 times larger than $B_s \rightarrow \phi K_s \rightarrow \phi\pi^\pm\pi^\mp$. There are 3 means to reject this background:

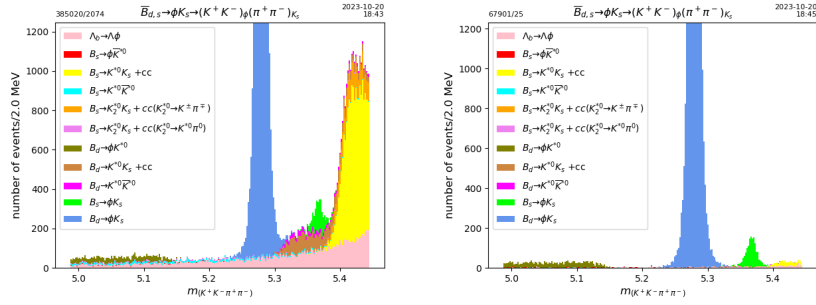


Figure 5: Reconstructed final states $\bar{B}_{d,s} \rightarrow \phi K_s$ for an integrated luminosity of 15 ab^{-1} at the Z-pole. In the left plot, no cut on the K^+K^- and $\pi^+\pi^-$ mass is applied. The right plot includes the cuts $1.00 \text{ GeV} < M_{K^+K^-} < 1.04 \text{ GeV}$ and $0.489 \text{ GeV} < M_{\pi^+\pi^-} < 0.506 \text{ GeV}$.

1. Requiring the $\pi^+\pi^-$ mass to be around the K^0 mass,
2. Eliminating events in which the combination of $\phi\pi^\pm$ is around the D_s^\pm mass,
3. Requiring the $\pi^+\pi^-$ pair to form a good vertex detached from the ϕ vertex.

We show the effects of cut 1 and cut 2 in Figure 6. The background $D_s\pi$ is completely eliminated with essentially no event loss for the signal.

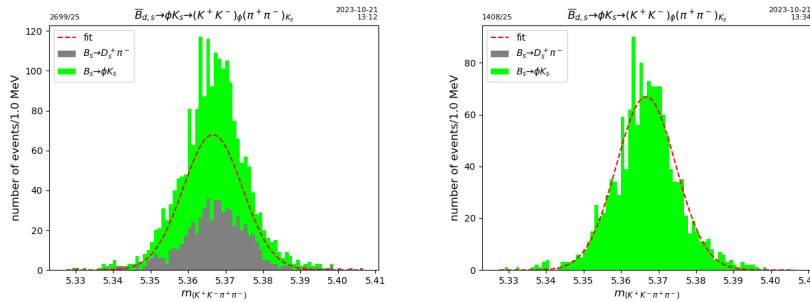


Figure 6: Reconstructed final states $\bar{B}_s \rightarrow \phi K_s$ for an integrated luminosity of 15 ab^{-1} at the Z-pole. In the left plot, cuts on the K^+K^- and $\pi^+\pi^-$ mass are applied but no cut on the $K^+K^-\pi^+$ and $K^+K^-\pi^-$ combinations. The right plot includes in addition the requirement that no combination $M_{K^+K^-\pi^\pm}$ is in the range $1.938 - 1.998 \text{ GeV}$.

5.2 Generic $b\bar{b}$, $c\bar{c}$ events

Therefore, the main source of background is expected to be of combinatorial origin. Inclusive Monte-Carlo samples of $Z \rightarrow b\bar{b}$ and $Z \rightarrow c\bar{c}$ events have been used to confirm this expectation, and to quantify the level of the combinatoric background. They consist of one billion of $b\bar{b}$ events, and of 500 millions of $c\bar{c}$ events, produced with the PYTHIA 8.306 Monte-Carlo generator [13]. Signal events are removed from the inclusive $b\bar{b}$ background sample. They are generated

separately, using PYTHIA to simulate the production of a $b\bar{b}$ pair in which one b quark hadronises into a B_d or B_s that decays into ϕK_s , while the other b -leg fragments and decays inclusively. The $B_{d,s} \rightarrow \phi K_s$ decay chain was performed with the EvtGen [14] program. The generated events were passed through a fast simulation of the IDEA detector [3], which provides resolutions similar to the ones given in Section 4.1. The simulation is based on DELPHES [10]. In particular, the simulation software that turns charged particles into simulated tracks relies on a full description of the geometry of the IDEA vertex detector and drift chamber. The software accounts for the finite detector resolution and for the multiple scattering in each tracker layer and determines the (non diagonal) covariance matrix of the helix parameters that describe the trajectory of each charged particle. This matrix is then used to produce a smeared 5-parameters track, for each charged particle emitted within the angular acceptance of the tracker. Finally, the events were subsequently analysed within the FCCAnalyses framework [15].

The reconstruction of signal candidates starts with the identification of the “primary tracks”, that can be fit to a primary vertex*, and, consequently, of the “secondary tracks”. Moreover, all reconstructed particles are used to determine the thrust axis, and the plane orthogonal to this axis and containing the interaction point divides each event in two hemispheres.

Pairs of opposite-charge secondary tracks that belong to a same hemisphere are fit to a common vertex. Pairs for which the vertex fit has a good χ^2 (a rather loose cut, $\chi^2 < 10$, being used here), and whose invariant mass (determined from the tracks’ momenta at the fitted vertex) is within 1.00 and 1.04 GeV (448 and 548 MeV) define ϕ (K_s) candidates. This set of cuts appears with the label “1” in Tab. 4, which summarises all selection criteria. Only K_s candidates that decay within 1.5 m from the interaction point are selected for further analysis (cut 2); this cut removes K_s candidates made of short tracks, prone to large measurement uncertainties. For pairs of ϕ and K_s candidates that belong to a same hemisphere (cut 3), a vertex is fit from the two tracks that make the ϕ candidate and from the trajectory of the neutral K_s . The standalone vertex fit algorithm [11] used in this analysis is available in the distribution of the DELPHES package, and its recent extension to allow neutral particles to be included in the fit is described in [12]. Pairs with an invariant mass between 5.33 and 5.41 GeV (5.24 and 5.32 GeV), and for which the normalised χ^2 of this latter vertex fit is smaller than 7.5, define B_s (B_d) candidates (cut 4). Events containing at least one such candidate are kept for further analysis.

In a first step, a perfect PID is assumed and the Monte-Carlo infor-

*A simple iterative algorithm is used here. In a first step, all tracks are fit to a common vertex, using a constraint given by the beam-spot size. The track that gives the largest contribution to the χ^2 of the fit is removed, and the remaining tracks are fit again. The procedure is repeated until the χ^2 contribution of each track is below a given cut.

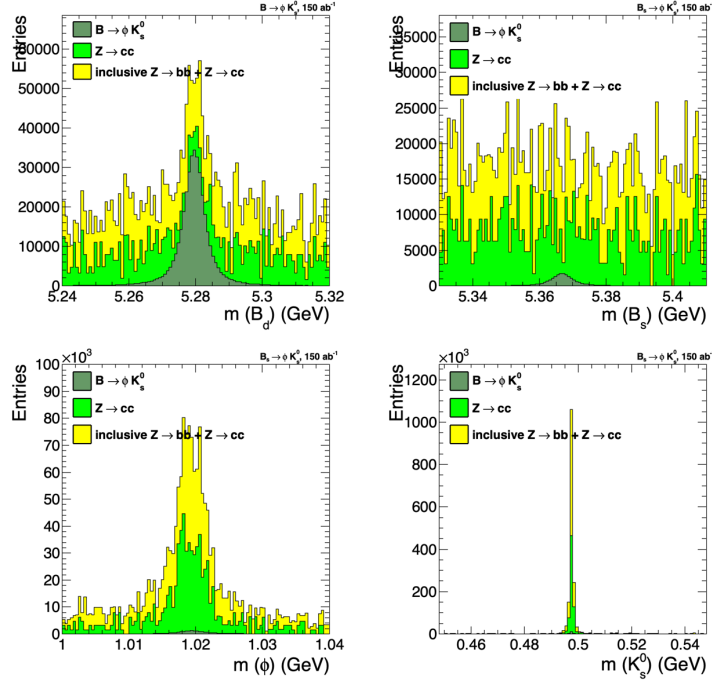


Figure 7: Top: Distribution of the mass of reconstructed B_d (left) and B_s (right) candidates prior to any selection cut. The histograms corresponding to the signal, to the $Z \rightarrow c\bar{c}$ background and to the $Z \rightarrow b\bar{b}$ background are stacked on top of each other. Bottom: Distribution of the mass of the ϕ candidate (left) and of the K_s candidate that make the B_s candidate.

mation is used to demand that the legs of the ϕ and K_s candidates that make the B candidate be kaons and pions, respectively (cut 5). At this stage, about 57% of signal events are selected, the loss being mainly due to the K_s acceptance. About 2 in 10^6 $b\bar{b}$ events contain a $B_{(s)} \rightarrow \phi K_s$ candidate, the rate for $c\bar{c}$ events being similar. The background is large compared to the signal, in particular for the small B_s signal, as shown in the top plots of Fig 7. The ϕ and K_s candidates that make B candidates are usually genuine ϕ and K_s particles, as shown by the lower plots of the same figure. The following cuts are applied to B_s candidates in order to suppress the background due to the exclusive processes considered in the previous section:

- the distance between the K_s decay vertex and the B_s decay vertex is required to be larger than 1 mm (cut 6);
- three-tracks vertex fits are run, from the two tracks that make the ϕ candidate and from each other track that belongs to the same hemisphere as the ϕ . If there is a track for which the resulting vertex has an acceptable χ^2 and a mass[†] below 1.986 GeV (the nominal D_s mass plus about twice the mass resolution), the B candidate is rejected (cut 7).

The latter cut efficiently removes $D_s \rightarrow \phi\pi$, $D_s \rightarrow \phi\mu\nu_\mu$ and $D_s \rightarrow$

[†]When determining the vertex mass, the track that does not come from the ϕ is given the pion mass, unless it comes from a muon or an electron, in which case the corresponding lepton mass is used.

$\phi e\nu_e$ events, as well as $D_s \rightarrow \phi\pi + X$ events, at the price of a relative efficiency loss of 15% on the signal. The mass distribution of the B_s

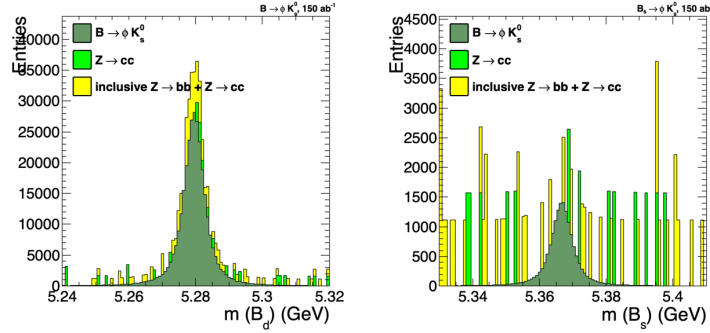


Figure 8: Distribution of the mass of reconstructed B_d (left) and B_s (right) candidates after the cuts designed against the exclusive processes considered in Section 5.1.

and B_d candidates passing these cuts are shown in Fig. 8. For the B_d signal, the purity is now quite good. The background contribution that is seen to peak at the B mass is due to $B \rightarrow f_0(980)K_s$ decays[‡], followed by a decay into K^+K^- of the $f_0(980)$. This contribution can be limited with a tighter lower cut on the mass of the ϕ candidate (cut (8a)). On the other hand, the much smaller B_s signal still suffers from a large background. It is clearly visible from the B_s mass plot that a much higher Monte-Carlo statistics would be needed in order to properly study the background. Assuming that the mass distribution of the background is flat in the range depicted in the plot, for an integrated luminosity of 150 ab^{-1} , about 11000 candidates are expected from $b\bar{b}$ background events under the B_s mass peak, with a 16% uncertainty, and about 5100 from $c\bar{c}$ events, with a 28% uncertainty. In comparison, 16000 signal candidates are expected for this luminosity. An investigation of the remaining background to the B_s signal confirms the combinatorial origin of the background at this stage; in the very large majority of the events, either the ϕ or the K_s is produced during the fragmentation, while the other meson is coming indeed from the decay of a heavy-flavour hadron. This background can be suppressed by kinematic cuts, since the mesons produced during the fragmentation are usually very soft (cuts 9). A loose cut on the momentum of the B_s candidate, and on the energy reconstructed in the signal hemisphere after removing that of the B_s candidate, also improves efficiently the signal-to-background ratio, as shown in Fig. 9 (cuts 10).

Another small component to the background comes from non-resonant decays $B_s \rightarrow K^+K^-K_s$, where the K^+K^- pair does not come from a ϕ meson; it can be further reduced with a tighter cut on the mass of the ϕ candidate (cut 8b).

The final selection cuts are summarised in Tab. 4. For simplicity, the same cuts (apart from the mass window) are used for selecting

[‡]With the default PYTHIA settings used here, the mass of the f_0 is set to 1 GeV and its width to 50 MeV. Both the width, and the branching fraction of the f_0 into K^+K^- , are actually very poorly known and, with the FCC data, the contributions from $B \rightarrow \phi K_s$ and from $B \rightarrow f_0 K_s$ will have to be fitted together.

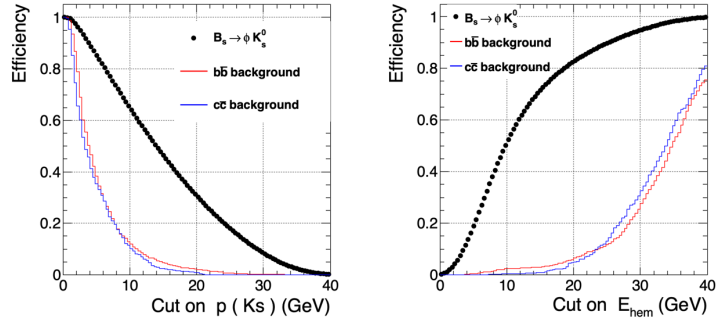


Figure 9: Efficiency of a lower cut on the B_s momentum (left) and of an upper cut on the energy reconstructed in the signal hemisphere after subtracting that of the B_s candidate (right). The dots show the B_s signal efficiency, and the red and blue lines the efficiency over $b\bar{b}$ and $c\bar{c}$ background events. The efficiencies are determined on top of the basic reconstruction criteria used in Fig. 7.

K_s leg:	(1)	vertex $\chi^2 < 10$
	(1)	$448 < m < 548$ MeV
	(2, 6)	flight distance > 1 mm and < 1.5 m
	(9)	$p > 1.5$ GeV
ϕ leg:	(1)	vertex $\chi^2 < 10$
	(1, 8a, 8b)	$1.01 < m < 1.03$ GeV
	(9)	$p > 1$ GeV
(5) perfect charged hadron PID for the K_s and ϕ tracks		
$B_{d,s}$ candidate:	(3)	the four tracks belong to the same hemisphere
	(4)	vertex $\chi^2 < 7.5$
	(4)	$5.24 < m < 5.32$ GeV for B_d
	(4)	$5.33 < m < 5.41$ GeV for B_s
	(10)	$p > 10$ GeV
Energy in signal hemisphere: (without the B candidate)	(10)	below 28 GeV
(7) no reconstructed $D_s^\pm \rightarrow \phi + \text{track} + X$ in signal hemisphere.		

Table 4: Summary of the final selection cuts used in this analysis. The labels allow to retrieve easily where the corresponding cuts are introduced in the text.

the B_d and the B_s signals (for the B_d , the aforementioned kinematic cuts further suppress the $c\bar{c}$ background). They result in an efficiency of 40% for both the B_d and B_s decays. The mass distributions obtained with this final selection are shown in the top row of Fig. 10. For the B_s selection, the $b\bar{b}$ background event that is observed right on the peak corresponds to a non-resonant decay $B_s \rightarrow K^+ K^- K_s$. Assuming that the mass distribution of the background is flat in the range depicted in the plot, about 1100 (400) $b\bar{b}$ ($c\bar{c}$) background events are expected under the B_s peak, with a 50% (100%) uncertainty, for 13400 signal candidates. Hence, despite the limited Monte-Carlo statistics, one can set a lower limit of about 5 on the signal-to-background ratio under the peak. Finally, the lower row of plots in Fig. 10 shows the distributions obtained when the PID requirement is not applied. One sees that PID capabilities are mandatory in order to extract the small B_s signal with a good signal-to-background ratio: without any PID, the background under the B_s peak would be as large as the signal.

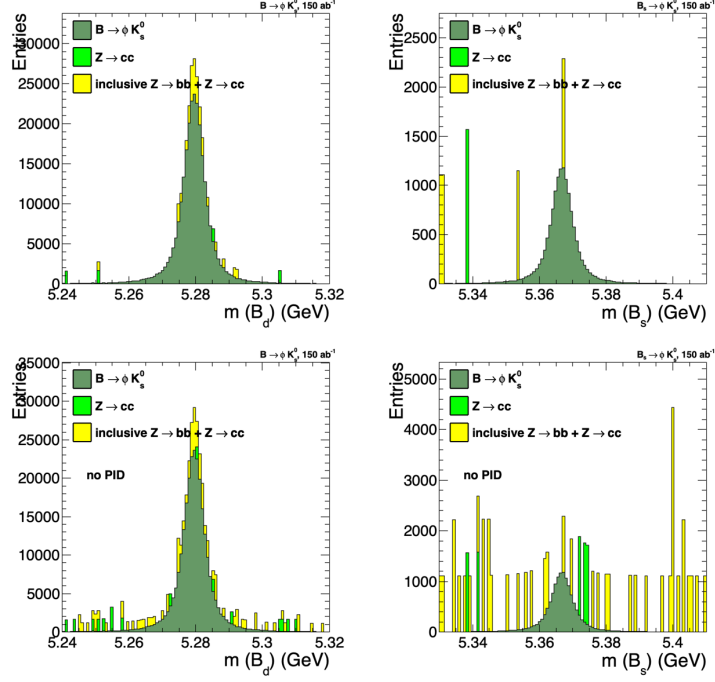


Figure 10: Distribution of the mass of reconstructed B_d (left) and B_s (right) candidates after the final selection cuts. The plots in the top row assume perfect charged hadron PID. The lower row of plots show the distribution obtained when no PID requirement is applied to the ϕ and K_s tracks.

6 Sensitivity to CP parameters

We have generated sets of events corresponding to the figures in Table 3 with their time dependence as written in equations (11) using the parameters in Table 2. The value of α_{ds} was set to 0.4 rad, which is close to the expected value from the SM.

In order to study the time dependence, one needs to identify the nature of the initial B meson (B or \bar{B}) decaying to $\phi K^{*0}(\bar{K}^{*0})$ at $t = 0$. This is done by tagging. The useful observed events are the tagged ones. Their time-dependent decay rate reads

$$\begin{aligned}
 \Gamma(\bar{B}_{tagged}(t) \rightarrow f) &= (1 - \omega)\Gamma(\bar{B}_q(t) \rightarrow f) + \omega\Gamma(B_q(t) \rightarrow f) \\
 \Gamma(B_{tagged}(t) \rightarrow f) &= (1 - \omega)\Gamma(B_q(t) \rightarrow f) + \omega\Gamma(\bar{B}_q(t) \rightarrow f)
 \end{aligned}
 \tag{25}$$

where ω is the fraction of wrong tagging. It is thus important to determine ω , since it damps the amplitude of the oscillations. The quality of tagging is quantified by the figure of merit $\epsilon(1 - 2\omega)^2$ shown in Table 5.

Let us define the time-dependent asymmetry :

$$\mathcal{A}_s = \frac{\Gamma(\bar{B}_{tagged}(t) \rightarrow f) - \Gamma(B_{tagged}(t) \rightarrow f)}{\Gamma(\bar{B}_{tagged}(t) \rightarrow f) + \Gamma(B_{tagged}(t) \rightarrow f)}
 \tag{26}$$

We show in Figure 11 the asymmetry as defined in equation (26). Obviously, one needs to measure ω precisely. Fortunately, this can be

Tagging Merit	LEP	BaBar	LHCb
$\epsilon(1 - 2\omega)^2$	25-30%	30%	6%

Table 5: Typical tagging Figure of Merit for some experiments. ϵ is the tagging efficiency and ω , the wrong tagging fraction, which is in the range $0 - 0.5$.

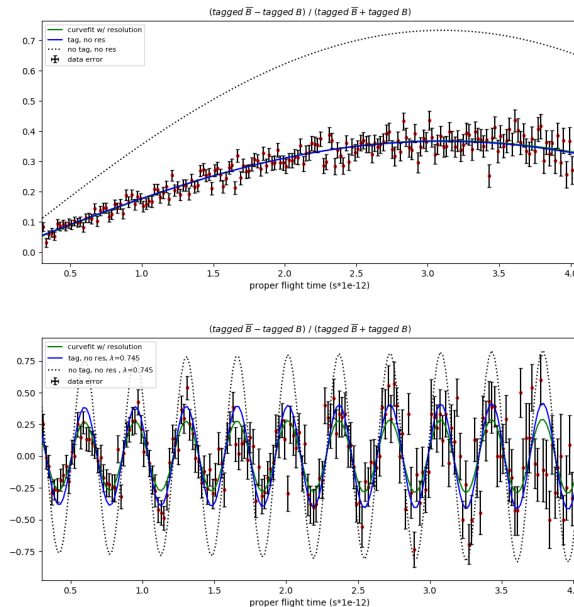


Figure 11: The B_d (top) and B_s (bottom) CP asymmetry for the events $\overline{B}_{d,s} \rightarrow \phi K_s$. The red points with error bars are the signal. The dotted line shows the asymmetry with $\omega = 0$. and no vertex resolution. The blue line corresponds to the asymmetry with $\omega = 0.25$ and no vertex resolution. The green line is the fit to the data.

done using the decay $\overline{B}_s \rightarrow D_s^+ \pi^-$. The method has been described in detail in [4]. Thanks to the large statistics at FCC, an uncertainty at the sub $\%$ level can be obtained for ω . In the following we have assumed conservatively $\omega = 0.25$ with negligible uncertainty and a tagging efficiency of 100%.

Figures 12 and 13 show the results of the fits for the values of λ_L and ϕ_L^{CKM} .

The sensitivities for the modes $\overline{B}_d \rightarrow \phi \overline{K}^0$ and $\overline{B}_s \rightarrow \phi K^0$, which one expects at FCC-ee, are summarized in Table 6.

One could improve the sensitivities in Table 6 by using also the final states with 2 vector particles however an angular analysis should be carried out in order to take full advantage of all events. A simpler way is to deal with the events as for pseudoscalar-vector decays. In that case, the CP asymmetry is further damped by the factor $\eta_f(f_{\parallel} + f_{\perp} - f_{\perp})$. For ϕK^{*0} , $\eta_f = +1$, hence, according to Table 1, the dilution factors are about 0.55 and 0.44 for $\overline{B}_d \rightarrow \phi \overline{K}^{*0}$ and $\overline{B}_s \rightarrow \phi K^{*0}$, respectively. The sensitivities for the modes $\overline{B}_d \rightarrow \phi \overline{K}^{*0}$

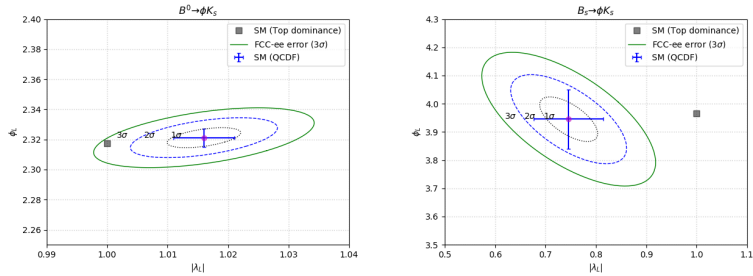


Figure 12: The sensitivities for the measurements of λ_L and ϕ_L (in radian) for $\overline{B}_{d,s} \rightarrow \phi K_s$.

Decay	$\sigma(\lambda_L)$	$\sigma(\alpha_{ds})(\text{rad})$
$\overline{B}_d \rightarrow \phi \overline{K}^0$	0.005	0.004
$\overline{B}_s \rightarrow \phi K^0$	0.039	0.045

Table 6: The expected sensitivities for λ_L and α_{ds} with the decays $\overline{B}_d \rightarrow \phi \overline{K}^0$ and $\overline{B}_s \rightarrow \phi K^0$.

and $\overline{B}_s \rightarrow \phi K^{*0}$, which one expects at FCC-ee (see Table 7), are significantly worse than for ϕK^0 because only $K^{*0} \rightarrow K^0 \pi^0$ decays can be used. A more complete analysis using the angular dependences of the polarization states would enable to improve the sensitivities by about a factor of 2 as displayed in the Figure 13.

Finally, it is very important to note that these modes require an outstanding electromagnetic calorimeter in order to get a manageable background both due to the combinatorics and, in the case $\overline{B}_s \rightarrow \phi K^{(*)0}$, from the decay $\overline{B}_d \rightarrow \phi \overline{K}^{(*)0}$, which would contaminate the former decay, should the photon resolution not be very good, more quantitatively $dE/E \leq 0.03/\sqrt{E(\text{GeV})} + 0.003$ is necessary.

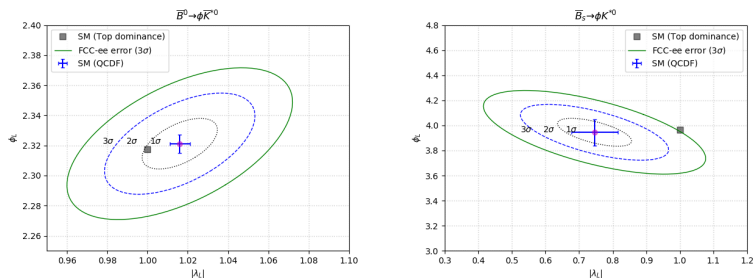


Figure 13: The sensitivities for the measurements of λ_L and ϕ_L (in radian) for $\overline{B}_d \rightarrow \phi \overline{K}^{*0}$ and $\overline{B}_s \rightarrow \phi K^{*0}$ assuming that an amplitude analysis disentangles the various polarisation configurations.

Decay	$\sigma(\lambda_L)$	$\sigma(\alpha_{ds})(\text{rad})$
$\overline{B}_d \rightarrow \phi \overline{K}^{*0}$	0.012	0.022
$\overline{B}_s \rightarrow \phi K^{*0}$	0.07	0.14

Table 7: The expected sensitivities for λ_L and α_{ds} with the decays $\overline{B}_d \rightarrow \phi \overline{K}^{*0}$ and $\overline{B}_s \rightarrow \phi K^{*0}$.

7 Conclusions

We have shown that it is possible to measure one of the angles of the flattest unitarity triangle, namely α_{ds} , using the decays $\overline{B}_d \rightarrow \phi \overline{K}^{(*)0}$ and $\overline{B}_s \rightarrow \phi K^{(*)0}$. Very interesting sensitivities, better than 4mrad, are expected at FCC-ee with an integrated luminosity of 150 ab^{-1} at a center of mass energy $E_{cm} = M_Z$ allowing one to perform further tests of the Standard Model. This measurement requires an excellent tracking system. In particular, a large tracking volume with many measurement layers is crucial for reconstructing K_s decays up to large flight distances, and a light tracker and a highly performant vertex detector are needed. Moreover, extracting the small B_s signal from the background requires charged hadron PID, and reconstructing the modes with a K^{*0} demands an outstanding resolution of the electromagnetic calorimeter.

Acknowledgments

We wish to thank Franco Bedeschi for making his vertexing code available and for very useful discussions about the reconstruction of displaced vertices.

References

- [1] M. Bicer, et al., *First look at the physics case of TLEP*, J. High Energy Phys. 01 (2014) 164, [https://doi.org/10.1007/JHEP01\(2014\)164](https://doi.org/10.1007/JHEP01(2014)164), arXiv:1308.6176.
- [2] A. Abada, et al., FCC Collaboration, *FCC Physics Opportunities : Future Circular Collider Conceptual Design Report Volume 1*, Eur. Phys. J. C 79(6) (2019) 474, <https://doi.org/10.1140/epjc/s10052-019-6904-3>.
- [3] A. Abada, et al., FCC Collaboration, *FCC-ee: The Lepton Collider : Future Circular Collider Conceptual Design Report Volume 2*, Eur. Phys. J. ST 228(2) (2019) 261, <https://doi.org/10.1140/epjst/e2019-900045-4>.
- [4] R. Aleksan, L. Oliver and E. Perez, *CP violation and determination of the bs “flat” unitarity triangle at FCCee*, Phys. Rev. D **105** (2022) 5, 053008 [arXiv:2107.02002[hep-ph]].
- [5] R. Aleksan, L. Oliver and E. Perez, *Study of CP violation in B^\pm decays to $\overline{D^0}(D^0)K^\pm$ at FCCee*, [arXiv:2107.05311[hep-ph]].
- [6] M. Kobayashi, T. Maskawa, *CP-Violation in the Renormalizable Theory of Weak Interaction*, Prog. Theor. Phys. **49** (1973) 652.
- [7] R. Aleksan, B. Kayser and D. London, *Determining the Quark Mixing Matrix From CP-Violating Asymmetries*, Phys. Rev. Lett. **73** (1994) 18-20, arXiv:hep-ph/9403341.
- [8] P.A. Zyla *et al.* [Particle Data Group], Prog. Theor. Exp. Phys. (2020) 083C01.
- [9] R. Aleksan and L. Oliver, in preparation.
- [10] J. de Favereau, C. Delaere, P. Demin, A. Giammanco, V. Lemaître, A. Mertens and M. Selvaggi, *Delphes 3: a modular framework for fast simulation of a generic collider experiment*, JHEP 2014 (Feb, 2014).
- [11] F. Bedeschi. Code available as part of the Track-Covariance module of the Delphes package, <https://github.com/delphes/delphes>.
- [12] F. Bedeschi. Presentation at the FCC Physics Performance meeting, October 2023, <https://indico.cern.ch/event/1337943/>.
- [13] C. Bierlich et al., *A comprehensive guide to the physics and usage of PYTHIA 8.3*, SciPost Phys. Codeb. 2022 (2022) 8, [arXiv:2203.11601[hep-ph]].
- [14] D. J. Lange, *The EvtGen particle decay simulation package*, Nucl. Instrum. Meth. A **462** (2001).
- [15] C. Helsens and the FCC software group, <https://github.com/HEP-FCC/FCCAnalyses>.